Sediment motion induced by Faraday waves in a Hele-Shaw cell

Román Martino,[1,2] Alejandro Boschan,[1,2] Diego Barba Maggi,[1,3] Gustavo Bongiovanni,[1] Jean-Christophe Géminard,[4] and Marcelo Piva[1]

[1]*Grupo de Medios Porosos, Fac. de Ingeniería, Universidad de Buenos Aires, Paseo Colón 850, (C1063ACV) Buenos Aires, Argentina*
[2]*National Scientific and Technical Research Council-Argentina (CONICET), Godoy Cruz 2290 (C1425FQB) CABA - Argentina, Argentina*
[3]*Escuela Superior Politécnica de Chimborazo, ESPOCH, Panamericana Sur Km 1 1/2, Riobamba, Ecuador*
[4]*Université de Lyon, Laboratoire de Physique, Ecole Normale Supérieure de Lyon, CNRS, UMR 5672, 46 Allée d'Italie, 96007 Lyon, France*

(Received 11 November 2019; accepted 1 April 2020; published 29 April 2020)

The interaction between the oscillatory boundary-layer flow induced by Faraday waves and a sedimentary granular layer was studied in a Hele-Shaw cell vertically vibrated. The experimental parameters were the vibration frequency f and acceleration a and the particle diameter d_p. At a critical value for the depth of the supernatant fluid layer Δh_c, a transition between a flat motionless granular layer and a second regime in which the granular layer undulates and oscillates periodically was observed. For the smallest value of d_p (for which the Stokes number was $\mathrm{St} \ll 1$) the reduced acceleration $\Gamma = a/g$ (g is the acceleration of gravity) is independent of Δh_c, while for the larger ones, Γ depends linearly on Δh_c. Finally, it is shown that at the onset of grain motion, the wave velocity $V_w = h_w f/2$ (h_w is the wave amplitude) depends linearly on Δh_c and is independent of d_p.

DOI: 10.1103/PhysRevE.101.043112

I. INTRODUCTION

The instability of a fluid layer in a vertically vibrated vessel, which manifests itself as a smooth, periodic, and stationary modulation of the free surface of the liquid, was first studied by Faraday [1]. Subharmonic, standing waves develop above a critical acceleration, under certain conditions, at half the driving frequency [2], which is characteristic of a parametric resonance. Faraday wave patterns depend on intrinsic properties of the system itself (the size and shape of the container and the viscosity, density, and surface tension of the fluid) and on the excitation frequency and amplitude. For nonviscous fluids, the phenomenon is explained in terms of the competition between the destabilizing vibration and the restoring effect of gravity and surface tension forces [3]. Linear analysis allowed researchers to extend theory to weakly viscous fluids and then to more dissipative systems [4–6]. Several experimental, analytical, and numerical works have shown that the damping of these waves originates in the viscous dissipation in the free surface, bulk, bottom, and side walls of the container. The damping coefficient introduced by dissipation depends explicitly on the layer thickness, as opposed to the inviscid case. Faraday waves have been studied extensively both experimentally and analytically since they constitute a basic flow instability problem in fluid mechanics [7]. They have also been used as a framework to investigate chaotic dynamics and to study transport phenomena in nonlinear systems.

There are many forms in which these waves can organize, and a great diversity of patterns has been reported in experiments, including, among others, squares, hexagons, and stripes. These spatiotemporal structures are directly related to the complexity in the presence of nonlinearity, and the available theoretical approaches, such as linear and weakly nonlinear theories, are insufficient to explain the physical phenomena involved in Faraday waves. Recently, very steep waves were reported to occur in Hele-Shaw cells [8–10]. These profiles with peak crests are distinct from traditional waves and indicate that the assumption of small amplitude cannot be applied. It was found that the sidewall proximity in small-scale containers can affect the deformation of the free surface significantly [11]. Numerical three-dimensional simulations of Faraday waves in containers with a narrow mouth were recently addressed with a novel model, the gap-averaged Navier-Stokes equations under the Poiseuille assumption of the velocity profile in the width [12], and validated by a series of laboratory experiments [13]. It was found that dispersion relations from linear theory fail in this case. The authors showed that the dimensionless wave height $h_w/\Delta h$ (h_w is wave height, and Δh is liquid depth) determines the extent of the nonlinearity: as $h_w/\Delta h$ decreases and $f/\sqrt{(a/\Delta h)}$ increases (f and a are forcing frequency and acceleration, respectively), the dispersion relations work well. Recently, the stability problem for Faraday waves in Hele-Shaw cells was addressed via a novel hydrodynamic model involving capillary action, capturing the variation of the dynamic contact line between two close walls, showing that the effect of the dynamic contact line is much greater than that of Poiseuille assumption [14]. Also recently, experiments were conducted in a Hele-Shaw cell to investigate the formation of Faraday waves in a triple layer of fluids (air, pure ethanol, and silicone oil) [15]. A system of two coexisting, strongly coupled waves at the two interfaces was observed: the upper waves (at the air-ethanol interface) vibrate vertically, whereas the lower ones (at the ethanol-silicone oil interface) oscillate horizontally. There is a threshold of the viscosity of the lower fluid (with the viscosity of the upper layer fixed within an appropriate range) for them to be observed. Results also suggests that the depth of the upper liquid plays a remarkable role, while the lower one does not seem to contribute significantly [16].

Faraday waves have been proposed as a template to generate particulate films on both the free surface [17] (relocation of floating particles) and the bottom of the container (sedimentary particles). A promising variety of applications make this subject an active field of research. For example, preferential particle deposition organized in a pattern has been reported under standing capillary waves [18] (Faraday waves in the limit of small wavelength, i.e., the restoring force is mainly the surface tension and gravity is negligible and in the thin liquid film approximation, i.e., the depth of the liquid is comparable to or smaller than the wavelength). The authors proposed using the induced oscillating boundary layers to control particulate deposition (powdered talc mixed with doubly deionized water) on the surface of the substrate. They found significant discrepancies between measured and predicted wavelengths for the particulate pattern. Based on prior works, they presume that a switch from a subharmonic instability to a harmonic instability occurs when the liquid layer gets sufficiently thin. But even under this hypothesis, the deviations at low frequencies remain unclear. Simulations of particle deposition beneath shallow, standing capillary waves showed that particles tend to accumulate at specific nodal regions beneath the waves and that the accumulation is maximized for an optimal particle diameter, which depends on the wave field, the fluid thickness, the particle density, and the fluid properties [19]. The development of bed forms in a thin sand layer covering the vessel bottom, in connection with experiments devoted to analyzing the effect of the secondary flows due to stationary circulatory flows in Faraday surface waves, was also reported [20]. Experimental results regarding the formation of stripes orthogonal to the direction of the periodic forcing, in horizontally oscillating granular suspensions, linked these patterns to the viscous shear stresses produced by the fluid and quantified this dependence via a Shields parameter defined for the flow configuration [21]. Any attempt to control and to impose a predefined pattern of granular material driven by Faraday waves must address the problem of the critical condition for the initiation of the grain motion. There is a lack of systematic results dealing with this issue, even when it is important in the study of stages prior to resuspension. Motivated by the above considerations, we conduct experiments in a Hele-Shaw cell in a system of two layers (the lower one is composed of granular material, and the upper one is a viscous liquid), with the aim being to investigate and document the onset of motion of settled particles due to the flow field induced by Faraday waves.

II. EXPERIMENTAL SETUP

The schematic of the experimental setup is shown in Fig. 1. A Hele-Shaw cell made of polymethyl methacrylate (PMMA), with inner dimensions of 152 mm (length) $\times$ 1.87 mm (width) $\times$ 75 mm (height) is attached to the axis of an electromagnetic shaker (Brüel and Kjaer, model V406) to provide the vertical vibration of the cell. The shaker is fed by a sinusoidal current from a power generator (MAXD, model 4210) driven by a function generator (GW-INSTEK, model 8219A). The resulting acceleration a is measured with an accelerometer (Analog Devices, ADXL325) attached to the body of the cell and monitored with an oscilloscope (GRATTEN, model GA1102CAL).

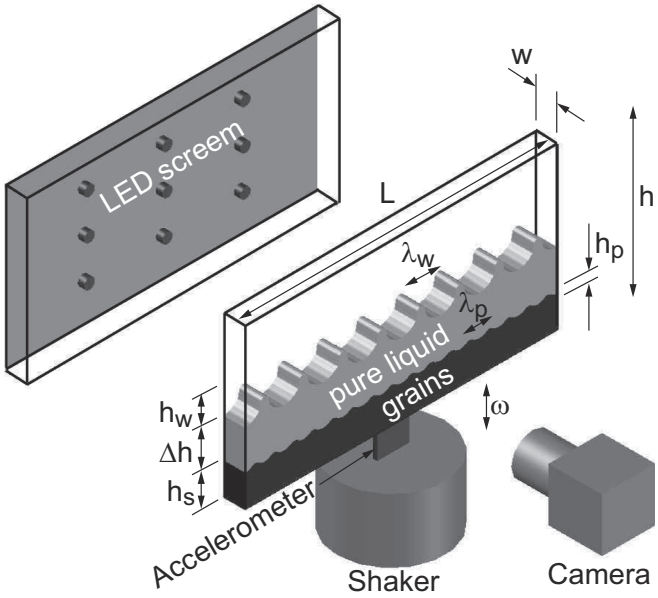

FIG. 1. Sketch of the experimental setup.

The cell is partially filled with a granular suspension made of monodisperse, spherical polystyrene beads of diameter $d_p = 40\,\mu$m and density $\rho_p = 1.05$ g/cm^3 immersed in a viscous fluid. The working fluid is a 20% ethanol-glycerin solution with density $\rho = 0.869$ g/cm^3, dynamic viscosity $\eta = 3.037$ mPa s, and surface tension, $\sigma = 22.5$ dyn/cm. As the ratio $w/d_p \approx 47$, a negligible influence of side wall friction on grain motion is expected [22,23].

Prior to the experiments, the suspension is allowed to settle for enough time that a flat layer of sedimented grains with a supernatant layer of clean fluid is obtained. The thickness of the sediment layer is set at $h_s = 10$ mm. We assume that the sediment forms a loose packing with a compacity $\phi \approx 0.58$ [24]. A light-emitting diode (LED) with a diffuser plate is used to get a uniform backlight illumination. Images of both the free surface interface and the sediment-fluid interface are obtained by a high speed camera (Basler A640-750 μm at 500 frames/s) with its optical axis perpendicular to the vibration plane. With this arrangement, the periodic character of the free surface profile is clearly identified, and the wave properties, such as their wavelength λ and the wave amplitude h_w, can be easily obtained by image processing.

III. EXPERIMENTAL RESULTS

In the first set of experiments, the threshold of Faraday instability was studied as a function of the reduced acceleration $\Gamma = a/g$, where g is the acceleration of gravity, for fixed frequency $f = 24$ Hz. The depth of the supernatant fluid was initially set at $\Delta h \approx 16$ mm, and the acceleration was gradually increased until a modulation of the free surface with finite amplitude was observed (the problem of hysteresis was not studied). The threshold acceleration Γ is then registered, and the procedure is repeated for a slightly smaller value of Δh, obtained by gently extracting with a syringe some

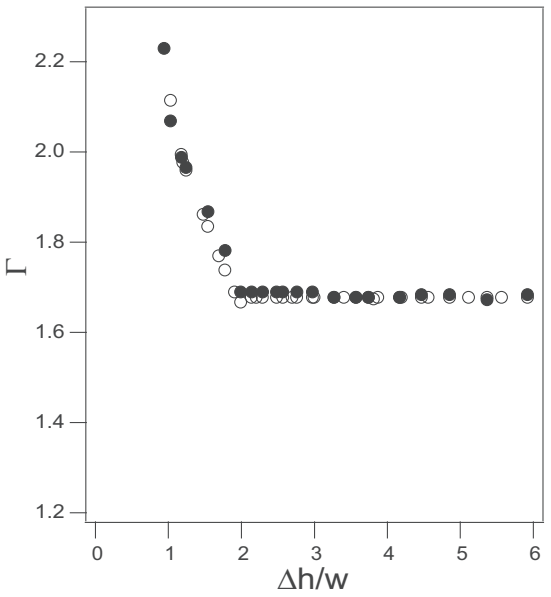

FIG. 2. Threshold of Faraday instability as a function of the reduced acceleration Γ and supernatant liquid depth Δh for $f = 24$ Hz. Open circles: only fluid. Solid circles: fluid plus particles.

ethanol-glycerol solution. Figure 2 shows the experimental threshold Γ (Δh, $f = 24$ Hz) measured with and without the granular layer (i.e., the smooth bottom of the cell).

It is observed that the threshold of the Faraday instability is not affected by the presence of the granular layer. Results also show the strong effect that the supernatant liquid depth Δh has on the acceleration threshold. This influence is remarkable in the range where Δh is comparable to w, indicating that the cell width is the appropriate length scale. Indeed, for vanishing $\Delta h/w$ the acceleration seems to approach infinity. On the other hand, for $\Delta h/w \gtrapprox 2$ ($\Delta h \gtrapprox 3.7$ mm) the reduced acceleration tends to an asymptotic value of $\Gamma \approx 1.66$, indicating that the threshold for Faraday instability becomes virtually independent of the fluid depth.

Observations for decreasing values of $\Delta h/w$ show that up to $\Delta h/w \simeq 3.86$ the bed remains flat (i.e., the granular layer behaves as if it were rigid). There are no observable grain motion or deviations from the flat profile. With the system far from the critical acceleration for which the grains begin to move due to vibration, it is concluded that with large Δh the secondary flow associated with the surface waves is not able to move grains since it is only significant over a depth of the order of the amplitude of the wave h_w, less than the total depth of the supernatant fluid layer Δh. Thus, a threshold or critical condition, for which the grains can be set into motion by the boundary layer of the wave-induced flow field, can be expected only for lower liquid depth.

Figure 3 shows a comparison of the wave half-cycle with the layer of motionless particles [snapshots in Fig. 3(a)] and without the granular layer [i.e., smooth bottom of the cell, Fig. 3(b)], with both experiments performed with the same liquid depth and forcing frequency and acceleration. As the wave patterns are identical in both configurations, it is concluded that the influence of the grains, if any, is quickly damped at a short distance from the bed, without affecting the development of the free surface instability.

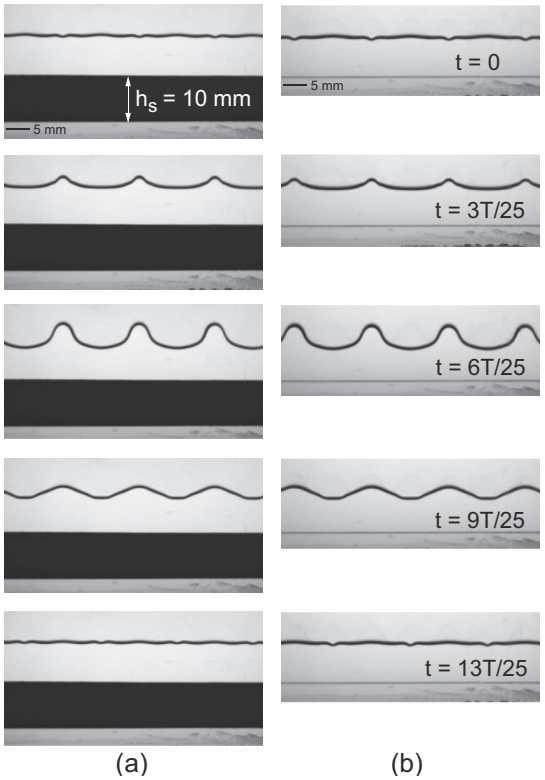

FIG. 3. Faraday waves patterns in half a cycle for $f = 24$ Hz, $\Gamma = 1.68$, and $\Delta h = 7.8$ mm: (a) with the granular bottom and (b) with a solid bottom. See Supplemental Material [25] for a video of Faraday waves.

A series of additional experiments was performed in this regime with motionless grains, as well as with the working liquid in the absence of the granular layer. Figure 4 presents the measurements in terms of the two dimensionless numbers first proposed by Li *et al.* [13], relating the height of the Faraday waves in the Hele-Shaw cell h_w, the liquid depth Δh, and the forcing frequency and acceleration, f and a, respectively. As can be observed, all points gather along a single curve, monotonically decreasing for $f/\sqrt{a/\Delta h}$ larger than 0.25 approximately. This result is coincident with those reported in [13], where the following functional relationship was proposed:

$$\log_{10}\left(\frac{h_w}{\Delta h}\right) = -\alpha\frac{f}{\sqrt{a/\Delta h}} + \beta, \tag{1}$$

with $\alpha = 1.21$ and $\beta = 0.51$ being fitting coefficients. Equation (1), plotted in Fig. 4 as a black dashed line, follows quite well our experimental points for $\alpha = 1.50$ and $\beta = 0.51$. The slight difference in the value of α is probably due to the fact that this coefficient depends on the cell dimensions and working fluid properties. A change in the trend of the curve is suggested for $f/\sqrt{a/\Delta h} < 0.25$. The change is also suggested in the previously cited work; the authors indicated that in this region dispersion relations from linear theory fail due to strong nonlinearities present in the flow field.

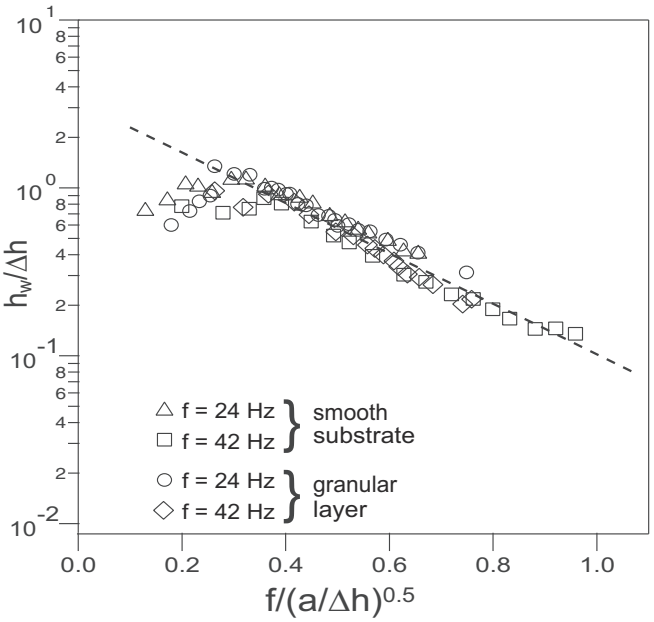

FIG. 4. The dimensionless wave height $h_w/\Delta h$ as a function of $f/\sqrt{a/\Delta h}$ for measurements above the layer of motionless grains and the acrylic bottom of the cell. Equation (1) is plotted as a black dashed line for fitting coefficients $\alpha = 1.21$ and $\beta = 0.51$.

Figure 5 shows the wavelength λ_w as a function of Δh, measured at the onset of the Faraday instability. Figure 5 also includes the theoretical curve for λ_w as a function of Δh, which can be explicitly obtained from the dispersion relation

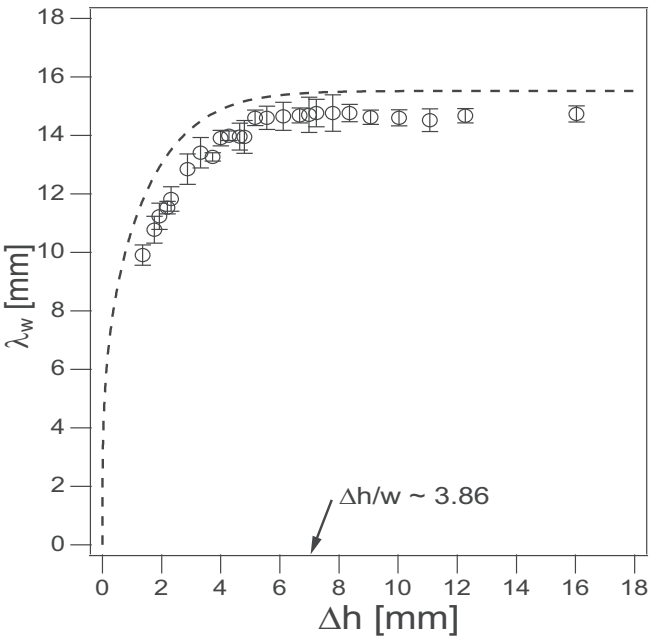

FIG. 5. Wavelengths of the Faraday waves as a function of Δh at the onset of Faraday instability for $f = 24$ Hz. The dashed line corresponds to the theoretical wavelength from the dispersion relation, Eq. (2), for a nonviscous fluid in an unbounded domain.

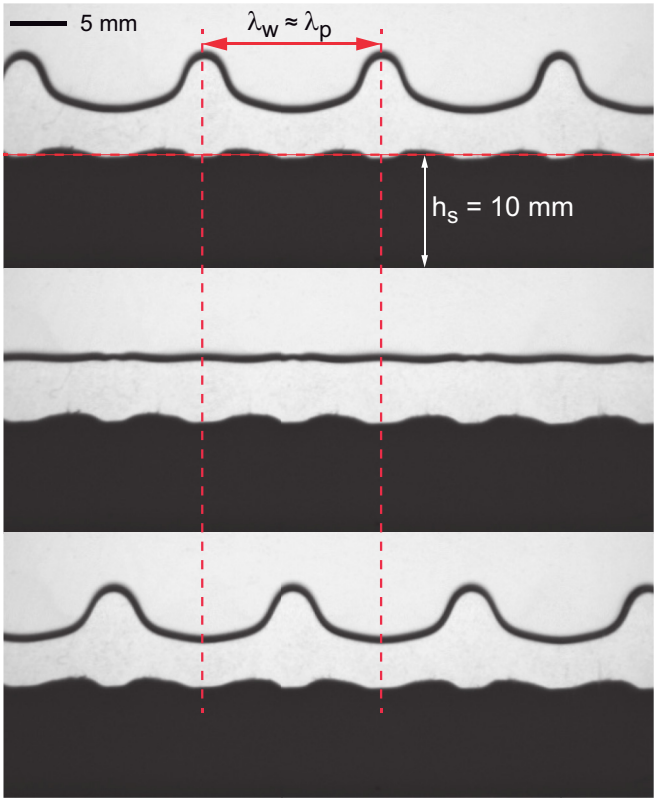

FIG. 6. Bed profiles at the Faraday threshold for $f = 24$ Hz and $\Delta h/w = 2.5$. See Supplemental Material [25] for a video of Faraday waves.

considering surface tension [7,11], which reads as follows:

$$f = \sqrt{\frac{2}{\pi \lambda_w} \tanh\left(\frac{2\pi \Delta h}{\lambda_w}\right)\left(\rho + \frac{4\pi^2 \Gamma}{\rho \lambda_w^2}\right)}. \qquad (2)$$

As can be observed, the trend followed by the measured points and the theoretical curve from Eq. (2) are quite close, as observed recently by Li *et al.* [11], indicating that the influence of the "rigid" granular bed on the wavelength turns out to be small even for small Δh. The persistent difference between experimental and predicted results is probably because Eq. (2) is obtained for an inviscid liquid in an unbounded domain. Shear viscous dissipation within the thin boundary layers developing in the sidewalls of the cell, separated from each other by the small cell width w, makes the flow field highly three-dimensional [13]. Because of the strong nonlinearities, the problem of determining the dispersion relation remains a challenging subject [10,11,13].

Observations of decreasing values of $\Delta h/w$ below $\Delta h/w \simeq 3.86$ revealed that the grain motion becomes evident and a periodic bed profile begins to develops. The evolution of the wave patterns for $\Delta h/w \simeq 2.5$ is shown in Fig. 6. The sequence shows that the granular bed undulates following the movement of the surface waves. Grains tend to move away from the zone of the wave troughs and migrate toward the position of the crests, in correspondence with the points of convergence of the secondary flow. Only at the instant when the free surface of the fluid becomes flat does the bed shape become approximately sinusoidal. But, in general, unlike

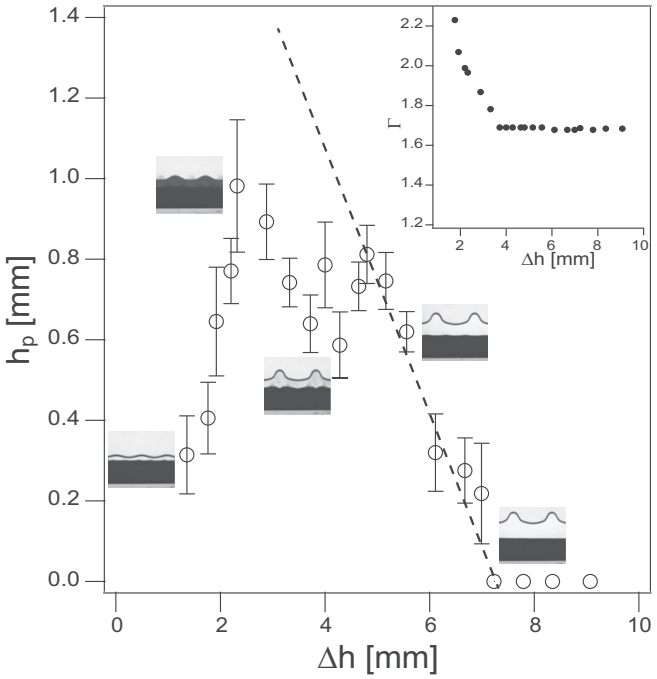

FIG. 7. The amplitude of the sediment profile wave h_p as a function of the supernatant liquid depth Δh for $f = 24$ Hz. The onset of sediment motion occurs at $\Delta h_c \simeq 7.1$ mm.

Faraday waves, each granular mound is asymmetrical when compared to its immediate neighbors due to the horizontal, oscillatory motion they perform. The granular wave exhibits spatial periodicity only by considering pairs of mounds. Thus, we adopted the length between pairs of mounds as the granular wavelength λ_p, whose value is very close to the corresponding Faraday wavelength above it. The troughs of the ripples remain in the same place (relative to the container). Thus, the dynamics of the whole system can be viewed as a lower granular wave, oscillating horizontally as induced by the upper Faraday waves, which develop in the liquid layer. The movies in the Supplemental Material show the details of such undulations. During the time span of the tests, the liquid layer remained clean, indicating that no particles were held in suspension. This means that the main transport mechanism is bed load, with grains driven back and forth by the oscillating boundary layer flow. This is indicative that the granular waves are excited by the upper vertically vibrating Faraday waves via viscous friction.

By image processing the whole set of runs, the amplitude of the sediment bed profile h_p was obtained at the onset of the Faraday instability. Figure 7 shows that h_p depends strongly on the liquid layer depth Δh. By decreasing Δh (starting from a large value where the sediment surface is flat with $h_p = 0$), it is found that there is a critical value from which h_p grows rapidly. From the intersection of the black dashed line drawn in Fig. 7 on the horizontal axis, the onset of grain motion is obtained. For the case $f = 24$ Hz, it gives $\Delta h_c \simeq (7.1 \pm 0.1)$ mm. Thus, this procedure provides an efficient and accurate method to identify and quantify the critical condition for initiation of motion. Moreover, it provides insight into the ability of the secondary flows to put grains into motion since the hydrodynamic forces acting on the grains depend on the flow velocity at the grain height, which is, in turn, a function of the fluid layer depth Δh.

Snapshots included in Fig. 7 offer a qualitative description of the several granular patterns observed for decreasing Δh. As explained above, for $5 < \Delta h < 7.1$ mm, the liquid layer remained clear, mounds were well defined, and the trend of the measured points (see the black dashed line) allowed quantifying the threshold of sediment transport. For $3.5 < \Delta h < 5$ mm, grains tend to accumulate in triangular ripples, and tongues of resuspended sediment were observed directed towards the points of maximum curvature of the Faraday waves. For $2 < \Delta h < 3.5$ mm, ripples became steeper, and tongues increased in size, darkening the liquid layer. Recalling the fast growth in Γ (see the inset in Fig. 7), for decreasing Δh (from $\Delta h \approx 4$ mm), it is concluded that a larger injection of energy in a lower liquid layer implies stronger secondary flows which can resuspend sediment. Measuring h_p was a difficult task in this range, with large uncertainties around each mean value, explaining the scattering of the data points. Finally, for $\Delta h < 2$ mm ($\Delta h/w \lesssim 1$), Faraday waves are not steep, and the curvature decrease is accompanied by no grain resuspension. These features seem to be related to the strong nonlinearity associated with steep wave profiles. Li *et al.* [11] recently pointed out the key role played by fluid inertia in the case of steep waves in narrow containers. They postulated the presence of a vortex sheet along the free surface. Vortices, symmetrically located at the crest tip, periodically change their direction and stretch the free surface down much faster than other places, explaining the large curvatures near the crest. Although a quantitative description of these observations is beyond the scope of the present contribution, we hypothesize for $2 < \Delta h < 5$ mm that these vortical structures interact with the granular bed, driving sediment resuspension. For $\Delta h < 2$ mm, the curvature of the waves decreases dramatically, and the vortices are not strong enough to resuspend sediment. On the other hand, for $\Delta h > 5$ mm, the strong vortices are far enough from the granular bed to make resuspension not possible.

An additional study was performed to observe the behavior of the grains inside the bulk of the granular layer below the liquid-granular interface. This was made from the analysis of a series of snapshots captured at the subharmonic frequency of surface waves. Since the wave pattern is stationary, any local displacement of the particles, relative to the others, produces a change in the local intensity of the transmitted light. These intensity fluctuations, measured by the standard deviation (STD) of the gray levels per pixel in the image stack, allow us to construct a map that shows the agitation or activity of the grains. On that map, the bright pixels correspond to areas of high grain activity, whereas dark areas reveal the stationary grains. Figure 8(a) shows the gray level (STD) map for $f = 24$ Hz, $\Gamma = 1.68$, $d_p = 250\,\mu$m, and $\Delta h = 4.7$ mm, where net sediment motion is observed and granular waves coexist with the driving Faraday waves. The map shows an important activity of the grains: at the surface, the grain motion is high and concentrates on a thin layer a few grains wide. Below that, the activity gradually decreases to increasing depths, until reaching the dark zone where no grain is set into motion. The penetration scale is much larger than the grain size (of the

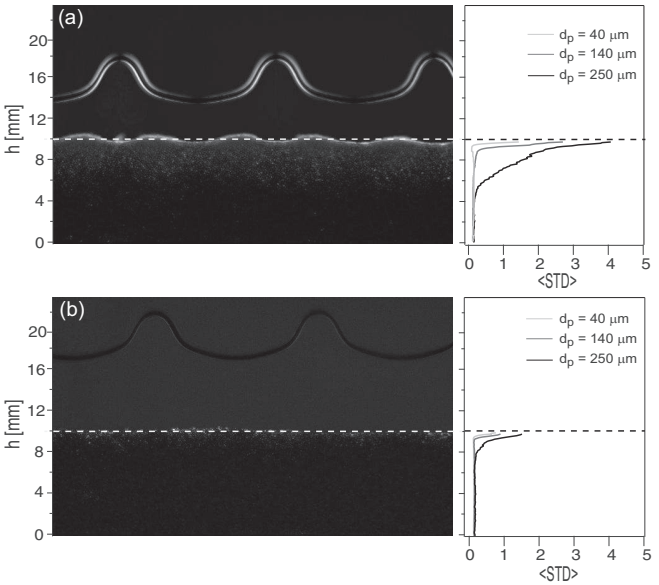

FIG. 8. Gray level standard deviation map, showing active zones of moving grains in the granular bed: (a) the active layer of sedimented particles shown below the Faraday waves extends over several grain sizes ($\Delta h = 4.7$ mm), and (b) below the threshold (for $\Delta h > \Delta h_c$) there are still waves, but no grain displacement is perceived ($\Delta h = 7.5$ mm).

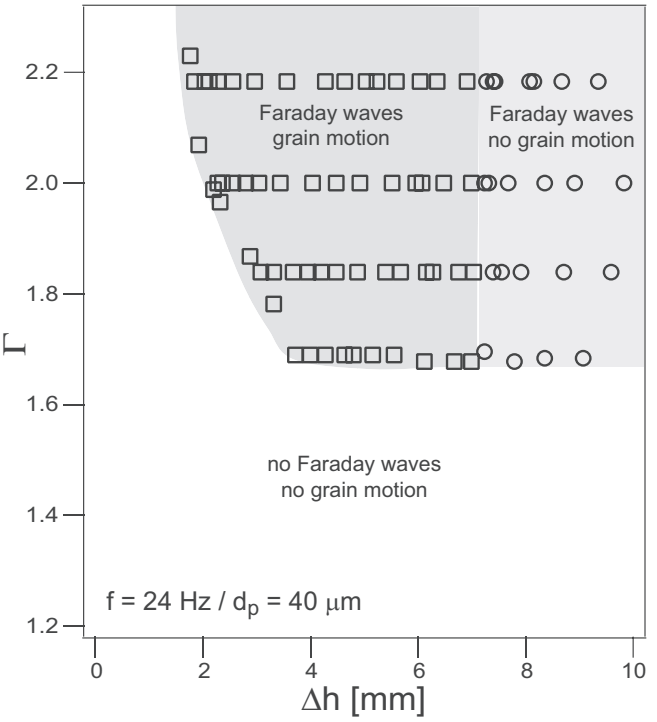

FIG. 9. Phase diagram in the parameters plane $\Gamma - \Delta h$ for $f = 24$ Hz and $d_p = 40\,\mu$m.

order of few millimeters), which suggests that the agitation of the grain is induced by strong shear stresses. At the right of the snapshot, the graph shows the averaged STD on horizontal lines versus depth inside the granular layer h. As can be observed, the penetration is quite small for $d_p = 40\,\mu$m and increases significantly as d_p increases.

Below the threshold of grain motion [$\Delta h > \Delta h_c \approx 7.5$ mm; see Fig. 8(b)], the map shows that grain activity is poor, even when there is a secondary flow above, induced by the surface wave. This is explained by the supernatant fluid layer being too wide and the shear stresses at the height of the grain-liquid interface not being enough to move the grains. That also means that the grains are not fluidized by the mere oscillation of the enclosure, which means that the injected energy into the grains through the enclosure border is not enough to overcome the large interparticle forces induced by lubrication. The light gray zones observed on the surficial layer of particles is due to grains trembling around their equilibrium position, departing from this location no more than $\pm d_p$, and no net transport of grains occurs. We can conclude that our criteria for determining the threshold of grain motion corresponds to Faraday waves that are able to transport grains far away from the equilibrium position of grains, thus giving rise to net sediment transport to well-defined troughs and crests in the granular surface.

By assuming that the results in Kiesgen de Richter *et al.* [24] (regarding the compaction dynamics of granular suspensions in a vertically vibrated cylindrical container) can be applied to the Hele-Shaw cell, the lubrication Péclet number was computed, $\mathrm{Pe} = \sigma_{lub}/(\mu P) \approx 1.6$. This number measures the competition between the lubrication stress (induced by vibrations) σ_{lub} and the granular pressure P (μ is the frictional intergrain coefficient). As expected, small values of both the diameter and the relative density of the grains lead to a large value of Pe. From Figs. 6 and 7 of Kiesgen de Richter *et al.*, the transition time (when the fast compaction stage is replaced by the slow one), $t_c \approx 25$ min, and the critical compacity, $\phi_c = \phi(t_c) \approx 0.65$, were obtained. Since our experiments lasted no more than 2 min, we assumed that any increase in ϕ would be small in this time span. Besides, compacity values are associated with the bulk of the granular column, whereas our measurements focused on the upper part of the sediment layer (at the interface with the supernatant liquid). Our observations (grain accumulation in oscillating mounds due to viscous shear stresses, with active zones of moving grains extending inside the bed over several grain diameters) allowed assuming that hydrodynamics forces are predominant in this region and that the influence of bed compaction could be neglected in a first approximation.

In addition to the previous ones, experiments were carried out to investigate the erosion threshold beyond the onset of Faraday waves. The procedure is similar to that used earlier: the liquid depth Δh was progressively decreased in each run, keeping the frequency fixed at $f = 24$ Hz but for a constant value of the acceleration, $\Gamma = cte$. The parameter plane $\Gamma - \Delta h$ (see Fig. 9) is divided into three different regions: a subcritical region where there are no Faraday waves or grain movement (white region), a supercritical one where there are Faraday waves but no grain motion (light gray region), and a third region where there are Faraday waves and significant bed surface grain activity, as is evident from the observation of well-defined, periodic bed profiles (dark gray zone). Note that the experiments cover the range $\Gamma < 2.3$. For larger accelerations, some effects due to the coupling of the fundamental

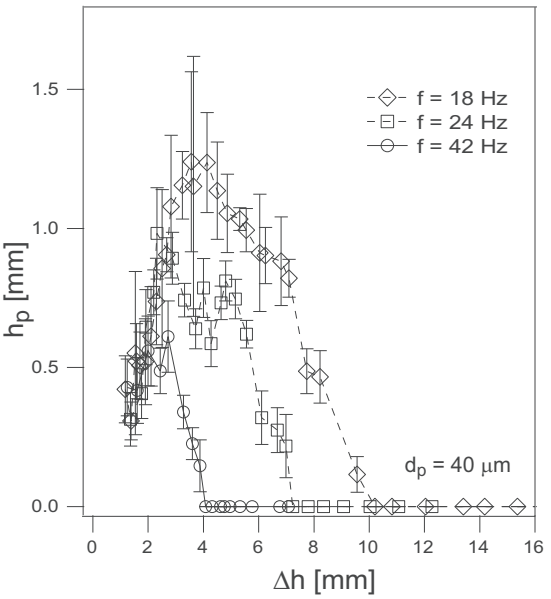

FIG. 10. Height of the sediment profile h_p as a function of the supernatant fluid layer Δh for three values of the forcing frequency f at the onset of Faraday waves.

with higher Faraday modes were observed, complicating the analysis of the problem. In addition, within the region of grain motion a subregion for small Δh was observed where particle resuspension takes place. This phenomenon is beyond the scope of the present article, but it is part of a current work that will be presented shortly.

From the phase diagram it appears that the threshold in Δh for sediment motion for $d_p = 40\,\mu$m is almost independent of Γ (the line between the light and dark gray regions is vertical in Fig. 9). This is an indication that inertia effects on the particle motion are negligible. Let's assume $V_w = h_w f/2$ (the product of the wave amplitude h_w and the frequency f of the first subharmonic wave at the onset of Faraday instability) is a suitable velocity scale for the secondary flow associated with the Faraday wave. The relative importance of the inertia of particles to the strength of the viscous drag can be estimated with the Stokes number $\mathrm{St} = \rho_p d_p/(18\eta)V_w$ [26], which for typical conditions of excitation frequency and acceleration ranges between 0.03 and 0.06; thus, $\mathrm{St} \ll 1$ for $d_p = 40\,\mu$m.

Another series of experiments was carried out to study the dependence of the onset of sediment motion on the excitation frequency f. The procedure was similar to that in the previous experiment: first, the onset of Faraday waves was found for a fixed frequency and varying Δh to give a curve $\Gamma(\Delta h, f)$, and then the critical value of Δh_c, for which some grains are observed to begin to accumulate, giving an undulating bed profile, was detected from plots of $h_p(\Delta h, f)$. For the purpose of illustration, plots of h_p vs Δh are displayed in Fig. 10 for three values of f. A summary of the obtained values of Δh_c and the associated parameters for the whole set of experiments is given in Table I.

From results reported in Table I, it can be seen that the larger the excitation frequency is, the smaller Δh_c is. Based on the moderate values of h_w/λ_w (wave steepness) and $h_w/\Delta h_c$

TABLE I. Critical values at the onset of particle motion for experiments at different frequencies at the threshold acceleration of the Faraday instability for grains of diameter $d_p = 40\,\mu$m.

f (Hz)	Γ	Δh_c (mm)	λ_w (mm)	h_w (mm)
14	1.36	13.6 ± 0.4	30.8 ± 0.7	12.0 ± 0.2
18	1.33	8.9 ± 0.7	22.8 ± 0.5	6.9 ± 0.1
24	1.69	7.1 ± 0.1	14.7 ± 0.5	4.4 ± 0.1
30	1.75	6.0 ± 0.1	11.2 ± 0.3	2.6 ± 0.2
36	1.78	4.5 ± 0.3	8.8 ± 0.3	2.0 ± 0.1
42	2.24	4.0 ± 0.1	7.5 ± 0.3	1.8 ± 0.1

in all runs, it is concluded that Faraday waves cannot be considered to have a small amplitude in these cases. By assuming V_w is an appropriate estimation of the intensity of the flow in the bulk of the cell above the granular layer and by plotting the critical depth Δh_c against V_w, it is shown that the points gather following a close to linear functional relationship (see Fig. 11).

Another set of experiments was performed to study the effect of particle size d_p on the critical conditions for the onset of grain motion. The procedure was the same as in the previous cases, and the threshold for initiation of motion was studied for particles of diameter 140 and 250 μm. The corresponding phase diagram in the plane $\Gamma - \Delta h$ for both grain diameters is shown in Fig. 12. It is observed that, for a given Δh, the larger d_p is, smaller the values of Γ need to be for the onset of the Faraday waves. This effect is remarkable on the threshold curves when d_p increases from 40 to 140 μm,

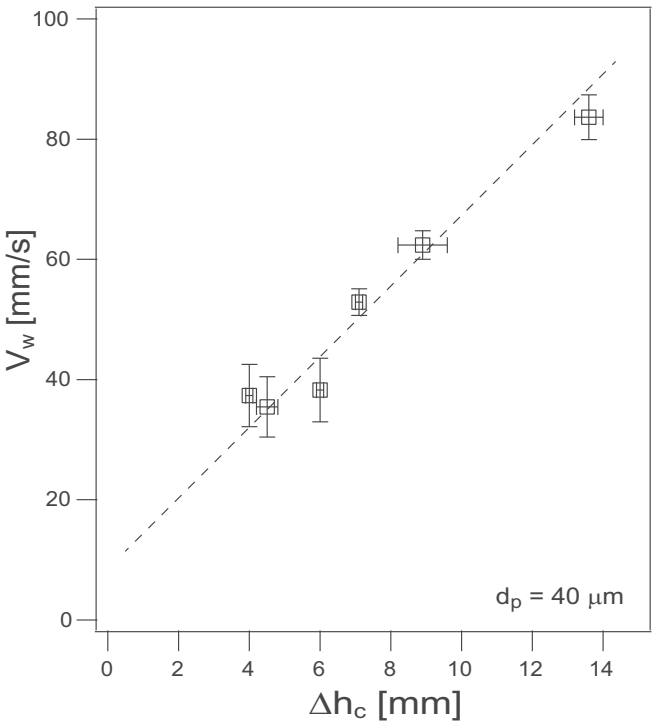

FIG. 11. Experimental relation between the depth of the supernatant liquid at the onset of grain motion Δh_c and the velocity scale based on the wave height, $V_w = h_w f/2$.

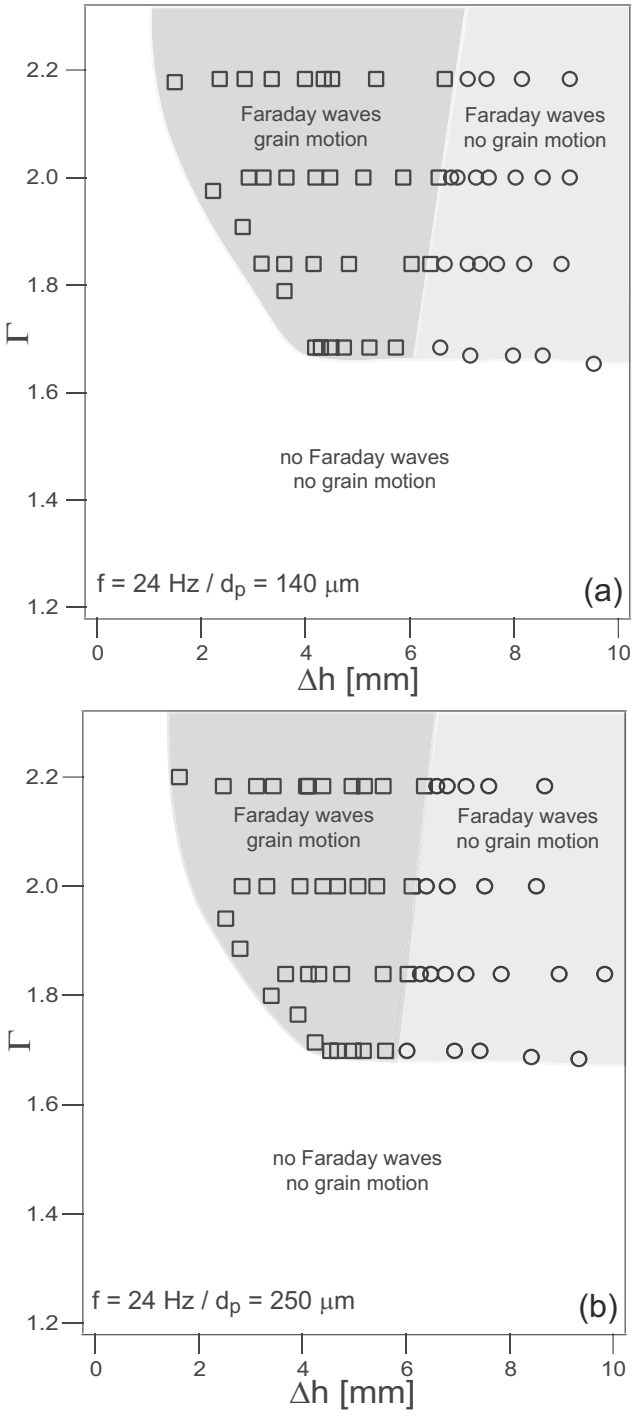

FIG. 12. Parameter plane $\Gamma - \Delta h$ for (a) $d_p = 140\,\mu$m and (b) $d_p = 250\,\mu$m.

but it is less noticeable when it further increases from 140 to 250 μm. This effect seems to be associated with the increase in the relative bed roughness. Let us assume that the viscous length $\delta = \sqrt{\nu/(\pi f/2)}$ provides a suitable metric for the thickness of the boundary layer in the Hele-Shaw cell. Since δ ranges between 200 and 300 μm for the explored values of f, it follows that the relative bed roughness defined as d_p/δ is of $O(10^{-1})$ for $d_p = 40$ μm, whereas it is of $O(1)$ for the bigger particles.

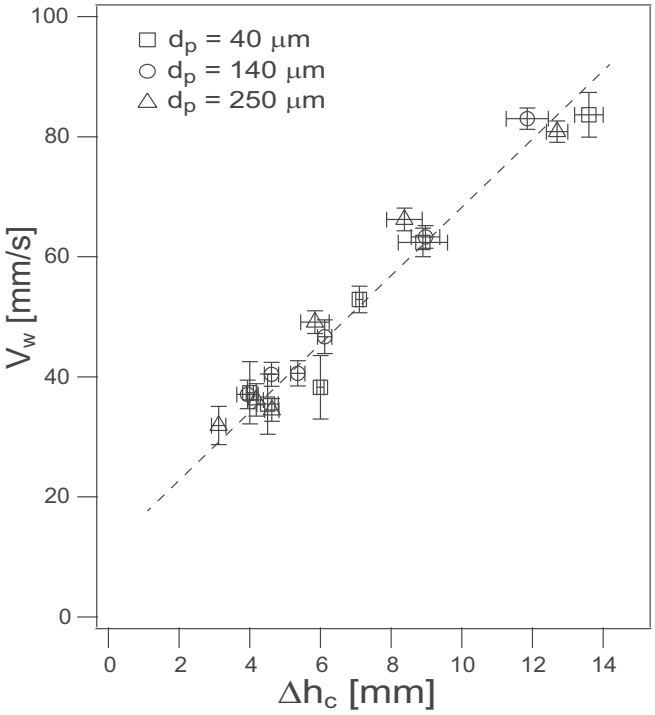

FIG. 13. Wave based velocity scale, $V_w = h_w f/2$, against the critical depth of the supernatant fluid Δh_c for different grain diameters d_p.

Regarding the onset of grain motion, as seen in Figs. 9 and 12, an almost linear dependence of Δh_c on Γ is observed for the larger particles, indicating inertia effects become important in the phenomenon. By plotting the computed values for V_w against Δh_c for 140 and 250 μm (see Fig. 13), it is worth noting that the points gather with those for 40 μm following a close to linear trend, virtually independent of d_p. The Shields number at the threshold of grain motion is $\theta^c = \eta\dot{\gamma}/(\Delta\rho g d_p)$, and the Reynolds number of the grain is given by $\mathrm{Re}_p = \rho\dot{\gamma}d_p^2/\eta$, with $\dot{\gamma}$ being the shear rate of the oscillating flow onto the bed. Assuming the slope of the straight line fitting data points in Fig. 13 is a suitable metric for $\dot{\gamma}$ and neglecting in the first approach the small y intercept (probably associated with the fact that the linear trend does not hold in the range $0 < \Delta h \leqslant w$, where the transition from steep to smooth wave profiles occurs), θ^c decreases from 0.4 to 0.04 as Re_p increases from 0.003 to 0.18. These values are comparable with results reported for the initiation of sediment motion under laminar flows [27]. Although somewhat crude, these results seem to indicate that a definition of viscous shear stress is appropriate to study the initiation of motion in this range. With the values of V_w the Stokes numbers for $d_p = 140$ μm and $d_p = 250$ μm range between $\mathrm{St} = 0.1$–0.2 and $\mathrm{St} = 0.2$–0.4, respectively. These moderate values, closer to 1 when compared to values for $d_p = 40\,\mu$m, confirm that inertia of the particles cannot be neglected in analyzing the onset of particle motion by Faraday waves. In contrast to the influence of grain size on the dependence of Δh_c on Γ, experimental results show that the increase in d_p does not impact the measured values for h_w and λ_w (see Fig. 14). Thus, for the values of d_p explored

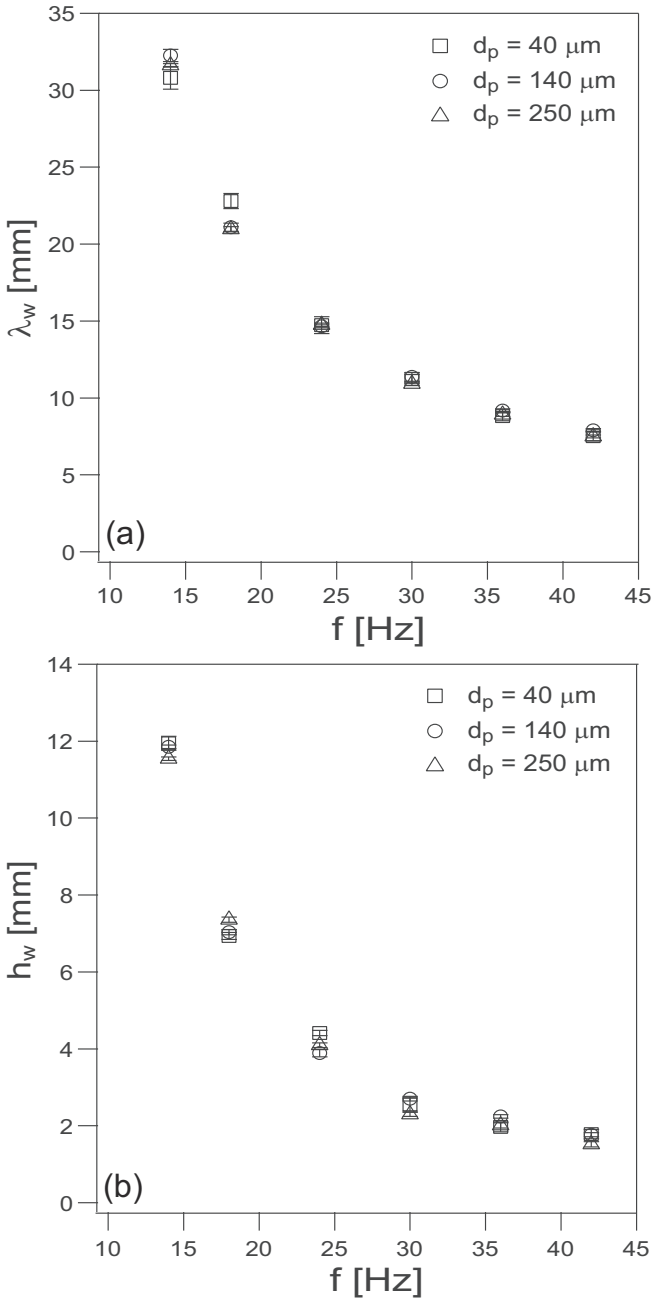

FIG. 14. (a) The length λ_w and (b) the amplitude h_w of the Faraday waves, measured at the onset of grain motions, as a function of the forcing frequency f and parameterized in d_p.

here, once a wave pattern is established at the free surface, the critical condition for initiation of grain motion at the bottom of the cell is reached without altering the structure of the wave.

IV. CONCLUSIONS

The critical condition for the onset of grain motion, driven by the oscillatory boundary-layer flow induced by Faraday waves in a Hele-Shaw cell, was experimentally studied for several values of forcing frequency f and acceleration $\Gamma = a/g$, as well as particle diameter d_p. In the presence of Faraday waves, two main regimes were identified in the plane of parameters $\Gamma - \Delta h$, with Δh being the depth of the supernatant liquid. In the first regime, the grains remain motionless, and the granular layer moves as a rigid boundary, whereas in the second regime, the granular layer undulates due to the appearance of a system of granular waves which oscillates horizontally, and the bed profile deforms in a rippled pattern with a well-defined amplitude h_p. The dynamic of the granular waves is closely related to the vertical Faraday waves above it, with the grains moving mainly as bed load in response to viscous forces.

The threshold condition for the initiation of grain motion can be precisely quantified from image processing, and results suggest that for small Stokes numbers, $\mathrm{St} \ll 1$, the critical values for Δh are almost independent of Γ, whereas a close to linear dependence between both variables can be inferred from the plane of parameters at moderate values of St (< 1), indicating that particle inertia becomes significant in defining the onset of sediment motion. In addition, it was also found that Δh_c depends almost linearly on the wave velocity $V_w = h_w f/2$, irrespective of the size of the grain d_p.

It was observed that an increase in particle diameter d_p alters the onset of the Faraday waves in the Hele-Shaw cell without significantly affecting the measured values for h_w and λ_w. This effect remains unclear, and further research is needed to clarify this finding. It seems to be related to the increase in the relative bed roughness d_p/δ, with δ being an estimator for the thickness of the oscillatory boundary layer. This is indicative that the flow structures expected to develop around the larger rough elements in the bed become important in the onset of the Faraday instability in the Hele-Shaw cell.

ACKNOWLEDGMENTS

The authors acknowledge the support from CAFCI and scholarships for university teachers awarded by SENESCYT-ECUADOR.

[1] M. Faraday, Philos. Trans. R. Soc. London **52**, 319 (1831).
[2] T. B. Benjamin and F. Ursell, Proc. R. Soc. London, Ser. A **225**, 505 (1954).
[3] J. Miles and D. Henderson, Annu. Rev. Fluid Mech. **22**, 143 (1990).
[4] K. Kumar and L. Tuckerman, J. Fluid Mech **279**, 49 (1994).
[5] K. Kumar, Proc. R. Soc. London, Ser. A **452**, 1113 (1996).
[6] E. A. Cerda and E. L. Tirapegui, J. Fluid Mech. **368**, 195 (1998).
[7] S. Douady, J. Fluid Mech. **221**, 383 (1990).
[8] J. Rajchenbach, A. Leroux, and D. Clamond, Phys. Rev. Lett. **107**, 024502 (2011).
[9] X. Li, D. Xu, and S. Liao, Phys. Rev. E **90**, 031001(R) (2014).
[10] X. Li, Z. Yu, and S. Liao, Phys. Rev. E **92**, 033014 (2015).

[11] X. C. Li, J. Li, X. M. Li, S. J. Liao, and C. H. Chen, Sci. China: Phys., Mech. Astron. **62**, 974711 (2019).
[12] P. Gondret and M. Rabaud, Phys. Fluids **9**, 3267 (1997).
[13] J. Li, X. Li, K. Chen, B. Xie, and S. Liao, Phys. Fluids **30**, 042106 (2018).
[14] J. Li, X. Li, and S. Liao, J. Fluid Mech. **871**, 694 (2019).
[15] X. Li, X. Li, and S. Liao, Phys. Fluids **30**, 012108 (2018).
[16] X. Li, J. Li, S. Liao, and C. Chen, Phys. Fluids **30**, 102103 (2018).
[17] G. Falkovich, A. Weinberg, P. Denissenko, and S. Lukaschuk, Nature (London) **435**, 1045 (2005).
[18] P. H. Wright and J. R. Saylor, Rev. Sci. Instrum. **74**, 4063 (2003).
[19] J. R. Saylor and A. L. Kinard, Phys. Fluids **17**, 047106 (2005).
[20] V. A. Kalinichenko and S. Ya. Sekerzh-Zeńkovich, Fluid Dyn. **43**, 125 (2008).
[21] R. Moosavi, M. Maleki, M. Reza Shaebani, J. C. Ruiz-Suarez, and E. Clement, Europhys. Lett. **107**, 34006 (2014).
[22] S. Courrech du Pont, P. Gondret, B. Perrin, and M. Rabaud, Europhys. Lett. **61**, 492 (2003).
[23] T. Loiseleux, P. Gondret, M. Rabaud, and D. Doppler, Phys. Fluids **17**, 103304 (2005).
[24] S. Kiesgen de Richter, C. Hanotin, P. Marchal, S. Leclerc, F. Demeurie, and N. Louvet, Eur. Phys. J. E **38**, 74 (2015).
[25] See Supplemental Material at http://link.aps.org/supplemental/10.1103/PhysRevE.101.043112 for videos accompanying Figs. 3 and 6.
[26] A. H. Clark, M. D. Shattuck, N. T. Ouellette, and C. S. O'Hern, Phys. Rev. E **92**, 042202 (2015).
[27] M. Ouriemi, P. Aussillous, M. Medale, Y. Peysson, and E. Guazzelli, Phys. Fluids **19**, 061706 (2007).